ACS Macro Letters

Letter

pubs.acs.org/macroletters

Morphology-Controlled Kinetics of Solvent Uptake by Block Copolymer Films in Nonselective Solvent Vapors

Anja Stenbock-Fermor,[†] Andrey A. Rudov,[†,‡] Rustam A. Gumerov,[‡] Larisa A. Tsarkova,*[,†] Alexander Böker,[†] Martin Möller,[†] and Igor I. Potemkin*[,†,‡]

[†]DWI – Leibniz-Institut für Interaktive Materialien, Aachen 52056, Germany

[‡]Physics Department, Lomonosov Moscow State University, Moscow 119991, Russian Federation

Supporting Information

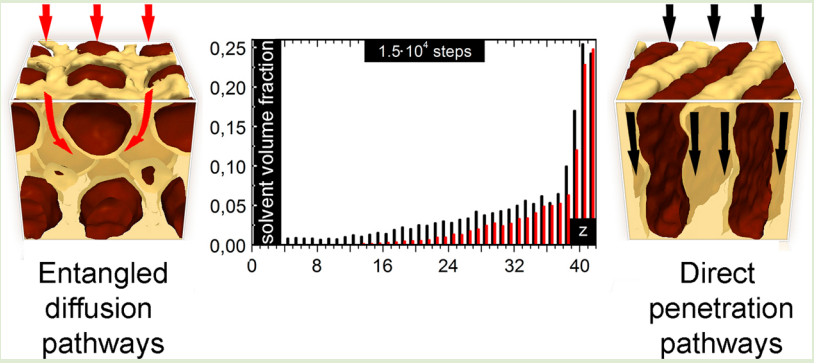

ABSTRACT: We compare the swelling behavior of a compositionally symmetric diblock copolymer in films with nonbulk micellar morphology and with vertically oriented lamellae. The morphologies preformed by spin-coating from selective/nonselective solvents differ in shape and total area of the AB interfaces between incompatible units. Experimental measurements and dissipative particle dynamics (DPD) simulations demonstrate that AB interfaces dominate as the diffusion pathways of nonselective solvent molecules in strongly segregated films. In experiments, the lamellar films swell about 20× faster as compared to densely packed micellar structures, while the degrees of swelling at saturation are equal for the two types of morphologies. The difference in the kinetics of solvent uptake vanishes as soon as the solvent plasticizing effect allows for micelles-to-lamellae transition. DPD simulations confirm the inhomogeneous distribution of the solvent inside the film, with the higher fraction of the solvent localized at the AB interface and reveal morphology-dependent kinetics of the solvent uptake. The effect of dissimilar abilities of the nanodomains and of AB interface to serve as diffusion pathways for small molecules may find potential in designing nanosensors and heterogeneous barrier layers.

Microphase-separated structures of block copolymers are characterized by extended internal interfaces between covalently linked incompatible blocks. The effect of the inhomogeneous distribution of a nonselective solvent in nanostructured concentrated solutions of diblock copolymers in a weak segregation regime was predicted decades ago.[1] Later on, this effect was detected experimentally by small-angle neutron scattering for the case of a neutral good solvent near the order–disorder transition.[2] The authors demonstrated that the fraction of the solvent localized at the AB interface is higher than that inside the domains. The partitioning of the solvent has a clear physical meaning: the energy of the unfavorable contacts at the AB interface can be diminished by the incorporation of solvent molecules.

Thin films of block copolymers exposed to solvent vapors may exhibit different behavior as compared to the bulk solutions due to the presence of confining surfaces and to the possibility of dynamic exchange with the solvent "reservoir" (vapor atmosphere). In particular, computer simulations[3] revealed that the lower the solvent concentration in the film, the more pronounced is the solvent redistribution between the interfacial regions and the domains.

Furthermore, Monte Carlo simulations revealed a clear enrichment of the interfaces between the incompatible units with free volume (voids).[4] Therefore, the AB interfaces are envisaged as potential nanochannels[5] to guide solution-diffusion pathways through nanostructured heterogeneous barrier layers.

Exposure of block copolymer films to the atmosphere of solvent vapors (solvent vapor annealing)[6] provides obvious technological benefits regarding the reduction of processing times and versatility of achievable morphological states.[7,8] However, the reproducibility and fine-tuning of the microphase separation behavior in swollen films is possible only under

Received: June 17, 2014
Accepted: July 31, 2014
Published: August 4, 2014

annealing protocols with precise control over the temperatures, as well as over the total and partial flows through the annealing chamber.[9,10] Also, an important control parameter is the swollen film thickness, which can be monitored in situ with, for example, optical reflectometry, ellipsometry,[10−12] or more advanced with grazing incidence small-angle X-ray scattering (GISAXS) allowing a direct access to the dynamics of the structural rearrangements.[13−17]

Here we report on the kinetics of the macroscale response of structured polymer films to the nanoscale effect related to diffusion pathways of small molecules. Specifically, we demonstrate that the swelling rate of a diblock copolymer film in a reduced atmosphere of nonselective solvent vapors depends on the block copolymer morphology. The observed effect is attributed to the inhomogeneous solvent distribution within the microphase separated structures, so that the ultimate swelling rate is determined by the overall area and the percolation pathways of the AB interfaces in the film.

We used a symmetric polystyrene-*b*-poly(2-vinylpyridine) diblock copolymer (denoted as SV) with a total molecular weight of M_n = 99 kg/mol and a characteristic lamellar spacing L_0 of 47.2 nm. The details on the synthesis using sequential living anionic polymerization and characterization of the SV sample are reported elsewhere.[11]

To guide the SV block copolymer into nonbulk core−shell spherical morphology, it was spin-coated from dilute solutions in toluene, a selective solvent for the polystyrene (PS) block (Figure 1a).[11,18] Vertically oriented disordered lamellar

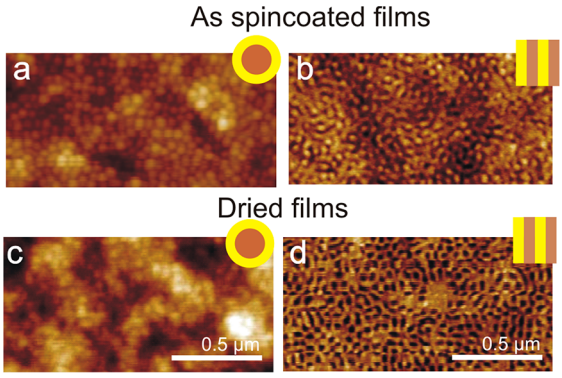

Figure 1. SFM topography images of SV films prepared from selective (a, c) and nonselective (b, d) solvents: ∼46 nm thick films in (a, c) have a nonbulk micellar morphology, while ∼60 nm thick films in (b, d) show a disordered upstanding lamellar phase. Films have been dried at elevated temperatures of 110 (c) and 70 °C (d) to remove the residual solvent. Both initial morphologies are preserved after the drying step. *Z*-scale is 5 nm.

structures are formed upon spin-coating from nonselective solvent (chloroform) as long as the film thickness is below 1.5 L_0 (Figure 1b).[19] SV films with micellar or lamellar structures, prepared as described above and specifically dried to remove the residual solvents, represent model nanoheterogeneous systems with different shapes and areas of the internal AB interface.

All samples have been exposed to the solvent vapor atmosphere using a custom-made liquid cell allowing controlling the temperature of the substrate and of the solvent vapor (21.0 and 20.0 °C, respectively) to ensure the reproducibility of the experimental conditions.[10] The solvent vapor treatment has been performed under a constant total flow of 100 sccm, while the partial vapor pressure of chloroform p/p_0 was adjusted by a defined combination of the flow of dry nitrogen and of the saturated chloroform vapor at isothermal conditions.[9−11,19] We assured fast vitrification of the structures by quenching the films using a flow of pure dry nitrogen. Experimental methods of measurements are described in Supporting Information.

Prior to the swelling experiments, SV films have been dried in vacuum at room temperature (RT) to remove the residual solvent. We found that this drying procedure was ineffective for the films with the micellar morphology. Fast evaporation of the residual solvent apparently did not allow eliminating air voids between randomly packed micelles as was evident from the ellipsometric measurements of the dried films. Instead of the slight decrease of the film thickness due to removal of the residual solvent, we systematically observed an increase of the thickness in 1−2 nm (2−3%) upon drying. Apparently, the voids between randomly packed micelles have been preserved or even enlarged due to the fast evaporation of the solvent in vacuum. To eliminate this extra free volume in the interior of the film, we preannealed films thermally at 110 °C (the boiling point of toluene). Since this processing temperature is just above the glass transition temperature of the PS, we additionally achieved a slight melting of micelles leading to filling-in the free voids, as could be seen from rather distorted shapes of the micelles in Figure 1c. Films with lamellar morphology have been preannealed at 70 °C which was sufficient to effectively eliminate the residual solvent (Figure 1d). Detailed comparative information on the drying regimes of the micellar films is presented in Figure S1 (Supporting Information).

Figure 2a shows the kinetics of the solvent up-take by SV films with micellar and lamellar morphologies, which have been subjected stepwise to the atmosphere of 20% of p/p_0 to achieve a constant level of the swollen thickness, and then to 40% of p/p_0. The swelling of the lamellae-forming film is fast, reaching the saturation within 5 min of exposure, in agreement with earlier observations.[11,19] The swelling kinetics of the film with the micellar morphology at 20% of p/p_0 is ∼20× slower as jugged from the time required to reach the saturation under given conditions state. However, the same degree of swelling of 1.12 is finally reached for both films. Although chloroform is almost a nonselective solvent for SV components[12] at a concentration of ∼10% in a film it provides a very limited plasticizing effect, so that after long-term annealing the micellar morphology is mostly preserved (Figure 2b-A). Also, lamellar structures in Figure 2b-B show almost no advancement in the long-range order as compared to as-spin coated films (Figure 1d).

Increasing the partial vapor pressure p/p_0 to 40% eliminates the differences in the kinetics of solvent uptake. Both films within 5 min achieve a similar value of saturated degree of swelling of 1.27. This observation can be explained by the analysis of the films morphologies. As shown in Figure 2b-C, after 10 min of exposure to the atmosphere of 40% of p/p_0 the micellar morphology is already transformed into up-standing lamella. Apparently, the transition proceeds simultaneously with the saturation of the film to solvent concentration of ∼30%. This effect can be attributed to the enhanced chain mobility, which is also evident by slightly improved lateral ordering of lamella structures (Figure 2b-D).

The results shown in Figure 2 suggest that solvent diffusion pathways in strongly segregated block copolymer films depend

dx.doi.org/10.1021/mz500347n | *ACS Macro Lett.* 2014, 3, 803−807

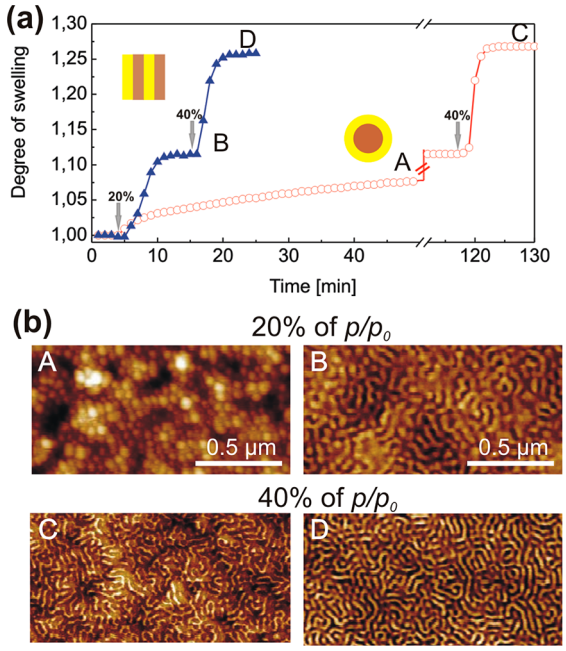

Figure 2. (a) Kinetics of the solvent up-take presented as degree of swelling (the ratio of the thicknesses of the swollen and dry film, h_{sw}/h_{dr}) upon stepwise saturation of the films with starting micellar (empty circles) and upstanding lamellar (solid triangles) morphologies at 20% and at 40% of (as indicated by arrows). (b) SFM topography images of the structures at the annealing stage indicated by a respective letter (A–D) in part (a). The annealing times are 1 h for the film in A and 10 min for the films in B–D.

on the block copolymer morphology and are dominated by the geometry of the AB interface. As shown in Figure S2 (Supporting Information), similar morphological effects on the kinetics of swelling are observed for thicker SV films. The figure suggests two additional observations. First, the kinetics of swelling of the film with the micellar morphology after drying in vacuum at RT is similar to that of lamellar structures, suggesting that air voids within such films ensure fast penetration pathways. Second, the lamellar structures in ∼130 nm thick SV films are predominantly oriented parallel to the film plane already during spin-coating. This orientation is dictated by selective interaction of the PVP block with the substrate and by lower surface tension of the PS block, which resides at the film–air interface.[20,21] However, the kinetics of swelling in a nonselective solvent seems to be insignificantly affected by the orientation of lamellae. We note that here we compare the swelling of nonequilibrated structures with high defect densities.

To get insights into the anomalously slow swelling of the films with spherical morphology and to follow the solvent penetration pathways, we employed DPD technique,[22−24] which earlier demonstrated its efficiency in studying solvent effects on the assembling of block copolymers.[3,25] To mimic the experimental preparation of the micellar films, we developed the following methodology (Figure S3, Supporting Information). Spherical micelles on the basis of nearly symmetric diblock copolymers[26−28] have been preformed in a selective solvent. Then, one of the micelles of the optimum structure was "cut out" from the simulated box and replicated. Next, identical micelles were packed into a dry film with symmetry of a body-centered cubic lattice and placed into a tetragonal box. The film preparation procedure and model of the solvent vapor are described in Supporting Information.

To preform lamellar morphology for the same block copolymer system, we started from spatially disordered state of the film and annealed it under dry conditions near the neutral substrate ($a_{AS} = a_{BS} = 50$, see Supporting Information). As a result, the perpendicular lamellae are formed,[20,29,30] Figure S3d. The whole set of the interaction parameters (Table S1), which were "switched on" at time $t = 0$ (exposition of the films to the solvent vapor), and the procedure to fix partial pressure is presented in Supporting Information.

The degree of swelling of the films as a function of simulation steps is shown in Figure 3. In the case of lower solvent

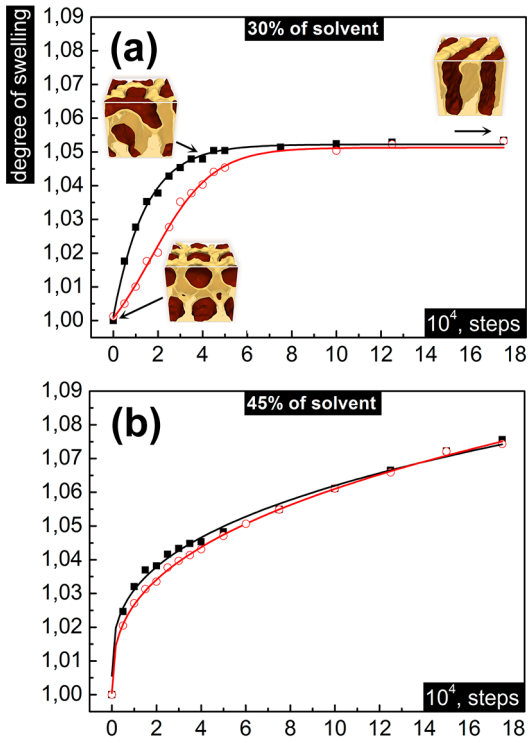

Figure 3. Degree of swelling (h_{sw}/h_{dr}) as a function of simulation steps for different values of the solvent concentration in the vapor: 30% (a) and 45% (b). Black squares and red circles correspond to lamellar and to micellar structures, respectively. Snapshots depict evolution of the morphology in the course of the film swelling: initial micellar structure at $t = 0$, transformation of the spheres after 4×10^4 steps, and perpendicular lamellae after 5×10^5 steps.

concentration (30%), one can observe a 2-fold delay in the swelling of the micellar morphology in the beginning of the swelling process (up to approx. 10^5 steps), Figure 3a. Similar to the experimental results in Figure 2a, equal degree of swelling of the films is achieved at saturation (plateau in Figure 3a). At a higher solvent concentration of 45% in the (chamber) atmosphere the difference in the swelling rates becomes less perceptible (Figure 3b) similar to the experimental observations in Figure 2a at 40% of p/p_0 when micellar structures transform into perpendicular lamellae. The simulated details of the morphology evolution are presented in Figure 3a. It should be noted that the micelles-to-lamellae transformation always occurs in computer simulations independently on the vapor concentration. This effect is a manifestation of equilibration of the system.

dx.doi.org/10.1021/mz500347n | ACS Macro Lett. 2014, 3, 803−807

The simulations assist to visualize the inhomogeneous distribution of the nonselective solvent inside the film and thus to assign the diffusion pathways of small solvent molecules to the film morphology. Figure 4a shows that a higher fraction

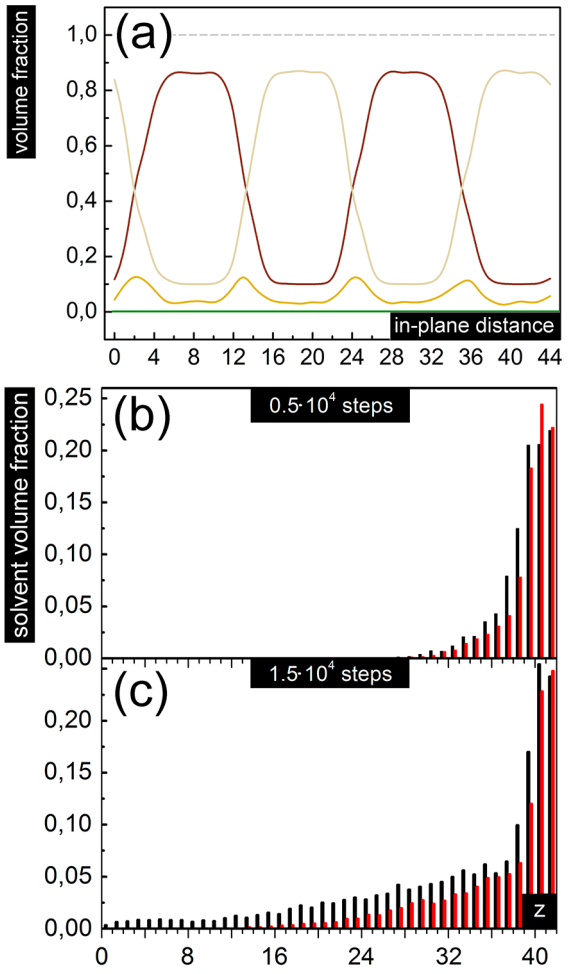

Figure 4. (a) Solvent (yellow) and polymer (brown and beige) volume fractions of swollen film as functions of lateral coordinate in the direction perpendicular to the lamellae after 4×10^4 simulation steps. The initial structure of upstanding lamellae in the dry film was equilibrium (Figure S3d). The solvent concentration in the vapor (30%) was kept constant. (b, c) Average volume fraction of absorbed solvent as a function of normal coordinate z after (b) 0.5×10^4 and (c) 1.5×10^4 steps. Black and red bars correspond to initial lamellar and micellar morphologies, respectively. The height of each bar is calculated as a ratio of the number of the solvent molecules in the corresponding layer to the total number of the solvent molecules in the film.

of the solvent is localized at the AB interfaces. This distribution was obtained for the film with initial lamellar structure swollen in 30% solvent vapor after 4×10^4 simulation steps. Therefore, the AB interfaces serve as more efficient diffusion pathways as compared to the domains. We argue that at low degrees of swelling there are two sorts of solvent diffusion-pathways in the course of the film swelling: along the AB interfaces and through the domains. The latter are less involved (the solvent concentration inside the domains is smaller than at the interfaces, Figure 4a) and are anticipated to be equal for both types of morphologies since the solvent is nonselective. We note that the overall AB interfacial area of the micellar structure is larger than that of lamellar for a given film volume. If we assume that the area of the interface per chain of the spherical micelle, which is formed in a strongly selective solvent, does not change during spin-coating and preannealing steps, one can estimate it as[26,31] $A_{mic} = 4\pi R^2/Q = 3N_B v/R \sim a^2(N_B/\gamma)^{2/5}$. Here the aggregation number Q of the micelle and the radius of the core $R \sim a\gamma^{2/5}N_B^{3/5}$ are connected through the dense-packing condition, $4\pi R^3/3 = QN_B v$, the monomer excluded volume v is related to the segment length a, $v \sim a^3$, and dimensionless core−solvent surface tension coefficient, $\gamma \sim 1$. In the case of the lamellar structure in the strong segregation regime, one can calculate $A_{lam} = N_B v/R \sim a^2(N_B/\gamma_0)^{1/3}$, where $R \sim a\gamma_0^{1/3}N_B^{2/3}$ is semithickness of the B-layer and γ_0 is the interfacial tension coefficient. Keeping in mind that $N_B \gg 1$, we get $A_{mic} > A_{lam}$. Therefore, interfacial diffusion pathways are longer and much more entangled in the micellar film as compared to the direct pathways in up-standing lamella-forming films. Furthermore, well-developed interfaces of the micelles deplete the intradomain flows which cross the AB interfaces more often (compared to the lamellar structure) and "lose" some amount of the solvent filling-in the interfaces. So, we can expect the upper layers of the micellar film to have higher swelling degrees than those of the lamellar film at the initial time, whereas the solvent penetrates deeper into the lamellar film. These effects are seen in Figure 4b,c, where the average solvent volume fraction is plotted as a function of normal coordinate z at different time points. Figure 4b demonstrates higher swelling of the upper layers (around z = 40) of the micellar film after 0.5×10^4 simulation steps and Figure 4c depicts distinct delay in the solvent penetration into micellar film after 1.5×10^4 simulation steps.

Disappearance of the differences in the swelling rates with the increase of the vapor density (45%, Figure 3b) might be related to the decrease of the difference in the concentration of the absorbed solvent at the AB interfaces and inside the domains: the solvent concentration profile in Figure 4a shifts upward.[3] As a result, the difference in the intensities of the interfacial and intradomain flows goes down and the swelling rate becomes independent of the film morphology.

Computer simulation results are qualitatively consistent with the experimental data. The quantitative difference in the swelling behavior between the experimental data and computer simulations is primarily related to much faster relaxation of metastable structures in DPD due to the fact that the blocks are always mobile ("liquid") in the film even without solvent and due to the ability of the chains to intersect each other (phantom chains). Also the difference in chain lengths plays a role.

In conclusion, we have demonstrated experimentally that the swelling kinetics of equivalent diblock copolymer films (formed by the same copolymer) in vapors of a nonselective solvent depends on the film morphologies. We propose explanation of the effect which is supported by DPD simulations. The dependence of the penetration rate of the nonselective solvent on the film morphology in strongly segregated systems is related to the inhomogeneous distribution of the solvent inside the film with the higher fraction of the solvent at the AB interfaces. Therefore, the interfaces are mainly responsible for the solvent diffusion upon the film swelling.

dx.doi.org/10.1021/mz500347n | ACS Macro Lett. 2014, 3, 803−807

■ ASSOCIATED CONTENT

Supporting Information

Experimental methods, Figures S1−S3, Table S1, and details of computer simulations. This material is available free of charge via the Internet at http://pubs.acs.org.

■ AUTHOR INFORMATION

Corresponding Authors

*E-mail: tsarkova@dwi.rwth-aachen.de.

*E-mail: igor@polly.phys.msu.ru

Notes

The authors declare no competing financial interest.

■ ACKNOWLEDGMENTS

The financial support of the Russian Foundation for Basic Research and the Deutsche Forschungsgemeinschaft within SFB 985 is gratefully acknowledged. The simulations were performed on multiteraflop supercomputers Lomonosov and Chebyshev at Moscow State University.

■ REFERENCES

(1) Fredrickson, G. H.; Leibler, L. *Macromolecules* **1989**, *22*, 1238−1250.

(2) Lodge, T. P.; Hamersky, M. W.; Hanley, K. J.; Huang, C.-I *Macromolecules* **1997**, *30*, 6139−6149.

(3) Rudov, A. A.; Patyukova, E. S.; Neratova, I. V.; Khalatur, P. G.; Posselt, D.; Papadakis, C. M.; Potemkin, I. I. *Macromolecules* **2013**, *46*, 5786−5795.

(4) Glagoleva, A.; Erukhimovich, I.; Vasilevskaya, V. *Macromol. Theory Simul.* **2013**, *22*, 31−35.

(5) Ma, H.; Burger, C.; Hsiao, B. S.; Chu, B. *ACS Macro Lett.* **2012**, *1*, 723−726.

(6) Sinturel, C.; Vayer, M.; Morris, M.; Hillmyer, M. A. *Macromolecules* **2013**, *46*, 5399−5415.

(7) Jeong, J. W.; Park, W. I.; Kim, M.-J.; Ross, C. A.; Jung, Y. S. *Nano Lett.* **2011**, *11*, 4095−4101.

(8) Kim, S. H.; Misner, M. J.; Xu, T.; Kimura, M.; Russell, T. P. *Adv. Mater.* **2004**, *16*, 226−231.

(9) Knoll, A.; Magerle, R.; Krausch, G. *J. Chem. Phys.* **2004**, *120*, 1105−1116.

(10) Zettl, U.; Knoll, A.; Tsarkova, L. *Langmuir* **2010**, *26*, 6610−6617.

(11) Gensel, J.; Liedel, C.; Schoberth, H. G.; Tsarkova, L. *Soft Matter* **2009**, *5*, 2534−2537.

(12) Olszowka, V.; Tsarkova, L.; Böker, A. *Soft Matter* **2009**, *5*, 812−819.

(13) Paik, M. Y.; Bosworth, J. K.; Smilges, D.-M.; Schwartz, E. L.; Andre, X.; Ober, C. K. *Macromolecules* **2010**, *43*, 4253−4260.

(14) Papadakis, C. M.; Di, Z.; Posselt, D.; Smilgies, D.-M. *Langmuir* **2008**, *24*, 13815−13818.

(15) Di, Z.; Posselt, D.; Smilgies, D.-M.; Papadakis, C. M. *Macromolecules* **2010**, *43*, 418−427.

(16) Di, Z.; Posselt, D.; Smilgies, D.-M.; Li, R.; Rauscher, M.; Potemkin, I. I.; Papadakis, C. M. *Macromolecules* **2012**, *45*, 5185−5195.

(17) Gu, X.; Gunkel, I.; Hexemer, A.; Gu, W.; Russell, T. P. *Adv. Mater.* **2014**, *26*, 273−281.

(18) Spatz, J. P.; Mössmer, S.; Hartmann, C.; Möller, M.; Herzog, T.; Krieger, M.; Boyen, H.-G.; Ziemann, P.; Kabius, B. *Langmuir* **2000**, *16*, 407−415.

(19) Stenbock-Fermor, A.; Knoll, A.; Böker, A.; Tsarkova, L. *Macromolecules* **2014**, *47*, 3059−3067.

(20) Potemkin, I. I. *Macromolecules* **2004**, *37*, 3505−3509.

(21) Potemkin, I. I.; Busch, P.; Smilgies, D.-M.; Posselt, D.; Papadakis, C. M. *Macromol. Rapid Commun.* **2007**, *28*, 579−584.

(22) Hoogerbrugge, P. J.; Koelman, J. M. V. A. *Europhys. Lett.* **1992**, *19*, 155−160.

(23) Koelman, J. M. V. A.; Hoogerbrugge, P. J. *Europhys. Lett.* **1993**, *21*, 363−368.

(24) Groot, D.; Warren, P. B. *J. Chem. Phys.* **1997**, *107*, 4423−4435.

(25) Rudov, A. A.; Khalatur, P. G.; Potemkin, I. I. *Macromolecules* **2012**, *45*, 4870−4875.

(26) Palyulin, V. V.; Potemkin, I. I. *Macromolecules* **2008**, *41*, 4459−4463.

(27) Erel, I.; Zhu, Zh.; Sukhishvili, S.; Patyukova, E.; Potemkin, I.; Kramarenko, E. *Macromol. Rapid Commun.* **2010**, *31*, 490−495.

(28) Venev, S. V.; Reineker, P.; Potemkin, I. I. *Macromolecules* **2010**, *43*, 10735−10742.

(29) Kellogg, G. J.; Walton, D. G.; Mayes, A. M.; Lambooy, P.; Russell, T. P.; Gallagher, P. D.; Satija, S. K. *Phys. Rev. Lett.* **1996**, *76*, 2503.

(30) Huang, E.; Rockford, L.; Russell, T. P.; Hawker, C. J. *Nature (London, U. K.)* **1998**, *395*, 757.

(31) Birshtein, T. M.; Zhulina, E. B. *Polymer* **1989**, *30*, 170.